

Spatio-temporal dynamics of wormlike micelles under shear

Lydiane Bécu*, Sébastien Manneville, and Annie Colin†
 Centre de Recherche Paul Pascal, Avenue Schweitzer, 33600 Pessac, FRANCE
 (Dated: March 22, 2022)

Velocity profiles in a wormlike micelle solution (CTAB in D₂O) are recorded using ultrasound every 2 s after a step-like shear rate into the shear-banding regime. The stress relaxation occurs over more than six hours and corresponds to the very slow nucleation and growth of the high-shear band. Moreover, oscillations of the interface position with a period of about 50 s are observed during the growth process. Strong wall slip, metastable states and transient nucleation of three-band flows are also reported and discussed in light of previous experiments and theoretical models.

PACS numbers: 83.60.-a, 83.80.Qr, 47.50.+d, 43.58.+z

Wormlike micelle solutions exhibit strong shear-thinning behavior due to the coupling between their microstructure and the flow. Along the steady-state flow curve (shear stress σ vs. shear rate $\dot{\gamma}$), a drop of up to three orders of magnitude in the effective viscosity $\eta = \sigma/\dot{\gamma}$ is observed in a very narrow stress range leading to a stress plateau (for a review, see Refs. [1, 2]). Such a sharp transition made wormlike micelle solutions appear as a model system to study shear-induced effects in complex fluids.

A partial understanding of the flow curve of wormlike micelles has emerged thanks to local scattering and velocimetry experiments. Above a critical shear rate $\dot{\gamma}_1$, a birefringent band normal to the velocity gradient occupies an increasing part of the gap as the shear rate is increased [3, 4]. This shear-induced birefringent band was clearly identified as a nematic phase in the case of concentrated solutions and has a low viscosity compared to the isotropic phase [3, 5]. Moreover, the velocity field was shown to separate into two differently sheared bands [6, 7]: a weakly sheared region flowing at $\dot{\gamma}_1$ and a highly sheared region at $\dot{\gamma}_2$, the upper limit of the stress plateau. In the well-documented system CPCl/NaSal in brine [8], the equilibrium position of the interface between the two shear bands increases linearly with $\dot{\gamma}$ consistently with the “lever rule” [6]. However, such a simple shear-banding scenario remains controversial due to (i) temporal fluctuations of the flow field and (ii) slow transients that question the existence of truly stationary states [7, 9, 10].

At this stage, due to the limited temporal resolution of current local velocimetry techniques (Nuclear Magnetic Resonance [7, 9, 10] and Dynamic Light Scattering [6]), a *time-resolved* description of the velocity field is still missing. In this Letter, velocity profiles obtained in cylindrical Couette geometry by high-frequency ultrasonic ve-

locimetry [11] and recorded every 2 s *simultaneously* to global rheological data are presented for a startup experiment followed over about six hours. For one of the much studied micellar systems (CTAB in D₂O), we show that two very different time scales are involved in the dynamics of shear banding. (i) A three-step nucleation and growth of a high-shear band occurs on a few hours. (ii) “Fast” oscillations of the band position with a period of about 50 s are pointed out. Subtle additional effects such as strong wall slip and transient nucleation of three-band flows are also reported and discussed.

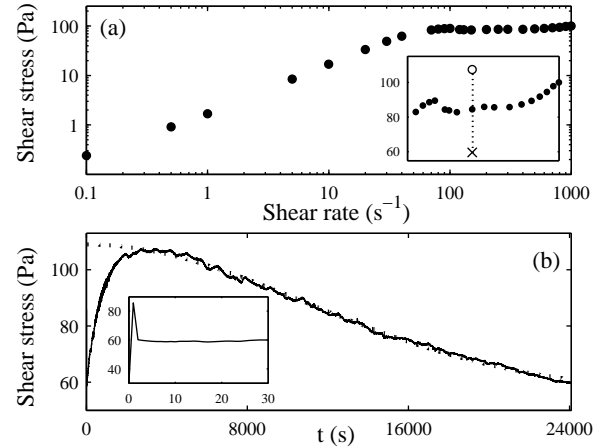


FIG. 1: (a) “Quasistatic” flow curve $\sigma(\dot{\gamma})$ obtained at $T = 44^\circ\text{C}$ under controlled shear rate (15 min per data point) by averaging the shear stress over the last 100 s of each step. Inset: enlargement over $\dot{\gamma} = 60\text{--}1000\text{ s}^{-1}$ showing the stress plateau. The dotted line corresponds to the stress response to a step-like shear rate from 0 to 200 s^{-1} . \circ and \times symbols indicate respectively the maximum and the last value of σ . (b) Temporal response of the shear stress $\sigma(t)$ after a step-like shear rate from 0 to 200 s^{-1} (thin line). The thick dotted line is the sigmoidal relaxation with $\sigma_\infty = 56.4\text{ Pa}$, $\sigma_M = 109\text{ Pa}$, and $\tau_{ss} = 15450\text{ s}$ (see text). Inset: enlargement over $t = 0\text{--}30\text{ s}$ showing the stress overshoot.

*Corresponding author: becu@crpp-bordeaux.cnrs.fr

†Present address: Rhodia Laboratoire du Futur, CNRS-FRE 2771, Bât. B de l’Institut Européen de Chimie et Biologie, 2 rue Robert Escarpiot, 33607 Pessac Cedex.

We focus on the salt-free wormlike micelle solution made of Cetyl Trimethyl Ammonium Bromide (CTAB)

at 20% wt. in deuterated water (D₂O) at a temperature of 44°C i.e. in the vicinity of the isotropic–nematic (I–N) transition that occurs at $T_{IN} = 39^\circ\text{C}$ [3, 9]. Rheological data are measured using a stress imposed rheometer (TA Instruments AR 1000) and a Couette cell of inner radius $R_1 = 24$ mm and gap width $e = 1.1$ mm. The cell is surrounded by a solvent trap containing water to prevent evaporation. Our local velocimetry technique is based on time-domain cross-correlation of high-frequency ultrasonic signals backscattered by the moving fluid. Post-processing of acoustic data allows us to record a velocity profile in 0.02–2 s with a spatial resolution of 40 μm (see Ref. [11] for more details). In order to enhance the scattering properties of our system, we add a small amount of colloidal particles (1% wt. polystyrene spheres of diameter 3 to 10 μm). We checked that the linear rheological properties as well as the plateau behavior were not significantly affected by the addition of those scatterers.

Using the shear rate imposed mode of the rheometer, we first apply increasing shear rates during a scanning time of 900 s per step. The resulting flow curve $\sigma(\dot{\gamma})$ shown in Fig. 1(a) presents a stress plateau at $\sigma^* \approx 84$ Pa that extends from $\dot{\gamma}_1 \approx 50$ s⁻¹ to $\dot{\gamma}_2 \approx 500$ s⁻¹ corresponding to a drop in the effective viscosity by an order of magnitude. Note that, in the system under study, the features of the plateau (σ^* , $\dot{\gamma}_1$, and $\dot{\gamma}_2$) depend dramatically on the scanning time as already reported in Ref. [3]. The bump in $\sigma(\dot{\gamma})$ revealed by the inset of Fig. 1(a) is characteristic of underlying metastable states [12]. Thus, between $\dot{\gamma}_1$ and $\dot{\gamma}_2$ and even for scanning times of 15 min, the flow curve of Fig. 1(a) does not represent true equilibrium states but rather describes qualitatively the plateau behavior of our system.

In the following, we apply a step-like shear rate into the plateau region from 0 to 200 s⁻¹ at time $t = 0$ and we record simultaneously the shear stress response $\sigma(t)$ and the velocity profiles for about six hours. As seen in Fig. 1(b), after an elastic overshoot during the very first seconds, $\sigma(t)$ increases from 60 to 105 Pa in 2000 s, then remains nearly constant at 107 Pa for 2500 s, and finally decreases very slowly for the rest of the experiment. This ultraslow decrease may be well fitted by a sigmoidal function $\sigma(t) = \sigma_\infty + (\sigma_M - \sigma_\infty) \exp((-t/\tau_{ss})^2)$ with $\tau_{ss} = 15450$ s and $\sigma_\infty = 56.4$ Pa [12]. Note that such a long equilibration time may be surprising for a wormlike micelle solution but is consistent with previous rheological data on the same salt-free system close to the I–N transition [3]. We checked that this very long time scale cannot be attributed to any evaporation effect by measuring the weight fraction of the sample before and after shearing using thermogravimetric analysis.

Figure 2 gathers the full ultrasonic velocimetry data on a spatio-temporal diagram of the local shear rate $\dot{\gamma}(x, t)$ calculated from the velocity $v(x, t)$ as $\dot{\gamma}(x, t) = -(R_1 + x) \frac{\partial}{\partial x} \frac{v(x, t)}{R_1 + x}$. The abscissae correspond to time t and the ordinates to the radial position x inside the gap

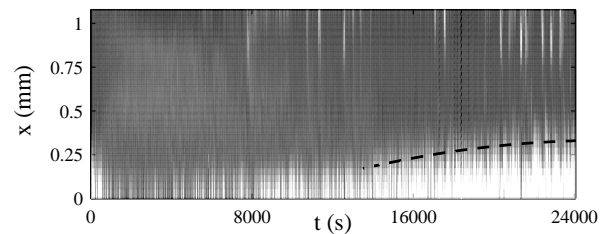


FIG. 2: Local shear rate $\dot{\gamma}(x, t)$. A linear gray scale is used: black and white correspond respectively to $\dot{\gamma} = 0$ s⁻¹ and $\dot{\gamma} \geq 300$ s⁻¹. The thick dashed line is given by $\delta(t) = \delta(t_0) + C \int_{t_0}^t (\sigma(t') - \sigma_\infty) dt'$, with $t_0 = 13500$ s, $\delta(t_0) = 0.17$ mm, and $C = 1.17 \cdot 10^{-6}$ mm Pa⁻¹ s⁻¹. $\sigma_\infty = 56.4$ Pa was deduced from Fig. 1(b).

of the Couette cell with $x = 0$ ($x = e$) at the rotor (stator). This representation reveals that the flow field slowly evolves in time but also undergoes “fast” fluctuations [13]. By first looking at the velocity profiles averaged over at most 6 min, we may distinguish three different regimes (indicated by arrows on Fig. 2 and summarized in Fig. 3) along the slow stress relaxation.

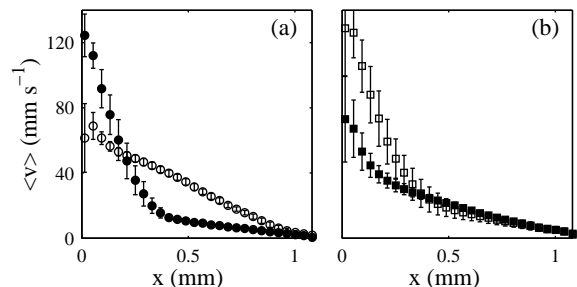


FIG. 3: Description of the slow dynamics. Velocity profiles $\langle v(x) \rangle$ averaged over (a) $t = 2$ –25 (●), 4400–4700 (○), (b) 12000–12230 (■), and 23600–23840 s (□). The error bars are the standard deviations of these estimates. The rotor velocity at $\dot{\gamma} = 200$ s⁻¹ is $v_0 = 196$ mm s⁻¹.

At the inception of the flow and for about 200 s, *two bands* bearing different shear rates, $\dot{\gamma}_h \approx 360$ s⁻¹ and $\dot{\gamma}_l \approx 16$ s⁻¹, coexist in the gap of the Couette cell (see ● symbols in Fig. 3(a)). The interface between the shear bands is located at $\delta \approx 0.3$ mm from the stator. Moreover, wall slip is present since the fluid velocity neither reaches the rotor velocity $v_0 = 196$ mm s⁻¹ at $x = 0$ nor perfectly vanishes at $x = e$. We define the slip velocities at the rotor v_{s1} and at the stator v_{s2} as the differences between the fluid velocity near the wall and the corresponding wall velocity, and get $v_{s1} \approx 75$ mm s⁻¹ and $v_{s2} \approx 3$ mm s⁻¹. Slip velocities are thus strongly dissymmetric and demonstrate that wall slip occurs preferentially in the low viscosity phase.

Second, after this first regime, the highly sheared band

disappears so that the bulk flow, when averaged over a few minutes, becomes *homogeneous* for about 8000 s. This regime is reminiscent of the “milky” turbid phase observed at “intermediate” times in Ref. [4]. Strong wall slip is detected at the rotor ($v_{s1} \approx 134 \text{ mm s}^{-1}$) while slip at the stator remains negligible (see \circ symbols in Fig. 3(a)). Note that the sliding layer at the rotor supports a very high shear rate of the order of 3000 s^{-1} and thus unambiguously differs from a band of nematic phase thinner than our resolution of $40 \mu\text{m}$ (that would flow at $\dot{\gamma}_h$). Another striking feature of this homogeneous velocity profile is the value of the “true” shear rate (calculated by removing the contributions of sliding layers) $\dot{\gamma}_{\text{true}} \approx 63 \text{ s}^{-1}$, which falls between the local shear rates $\dot{\gamma}_h$ and $\dot{\gamma}_l$ measured previously in the high- and low-shear bands. For such a shear rate, the flow is expected to show (at least) two shear bands. This suggests that during this part of the experiment, the system explores a metastable branch of the flow curve located above the stress plateau at σ^* [12]. Indeed, this second stage roughly corresponds to the increase and stagnation of the stress response $\sigma(t)$ well above both the asymptotic value $\sigma_\infty = 56.4 \text{ Pa}$ and the “quasistatic” plateau value $\sigma^* \approx 84 \text{ Pa}$ (see Fig. 1).

Finally, from $t \approx 8000 \text{ s}$ until the end of the experiment, the velocity profiles show the *growth* of a low viscosity layer in the vicinity of the rotor (see Fig. 3(b)) qualitatively similar to the “long” time behavior reported in flow birefringence experiments [4]. This highly sheared band expands until it fills roughly one third of the gap. During this growth stage, the slip velocity v_{s1} decreases from 134 to 64 mm s^{-1} so that the local shear rate in the high-shear band $\dot{\gamma}_h$ remains roughly constant and equal to 360 s^{-1} . Moreover, the weakly sheared band bears a constant local shear rate $\dot{\gamma}_l \approx 30 \text{ s}^{-1}$. Thus, although the asymptotic state is still not perfectly reached, the interface position at the end of the experiment is compatible with the lever rule: $\delta = (\dot{\gamma}_{\text{true}} - \dot{\gamma}_l) / (\dot{\gamma}_h - \dot{\gamma}_l) e \approx 0.3 \text{ mm}$.

Let us now get a closer look at the fast dynamics superimposed to the slow evolution described above. In the regime where the flow appears homogeneous on average ($t \approx 200\text{--}8000 \text{ s}$), Fig. 4(a) and (b) reveal that a thin band of width $\delta \lesssim 150 \mu\text{m}$ is actually nucleated and destroyed within short intervals of a few seconds unevenly every 5 to 20 s. When present, the band is sheared at $\dot{\gamma}_h$ and can be clearly distinguished from wall slip. Ref. [4] also reports the presence of a small shear band at the rotor as the “milky” phase disappears during the second regime.

Moreover, Fig. 4(c) and (d) show that, during the expansion of the highly sheared band ($t \approx 8000\text{--}24000 \text{ s}$), the interface is in fact subjected to periodic oscillations with a period of 50 s. As Fig. 5 points out, the slip velocity $v_{s1}(t)$ oscillates in phase opposition to the interface position $\delta(t)$, whereas the true shear rate $\dot{\gamma}_{\text{true}}(t)$ is synchronized with $\delta(t)$. These oscillations sometimes give way to the nucleation and destruction of a second highly

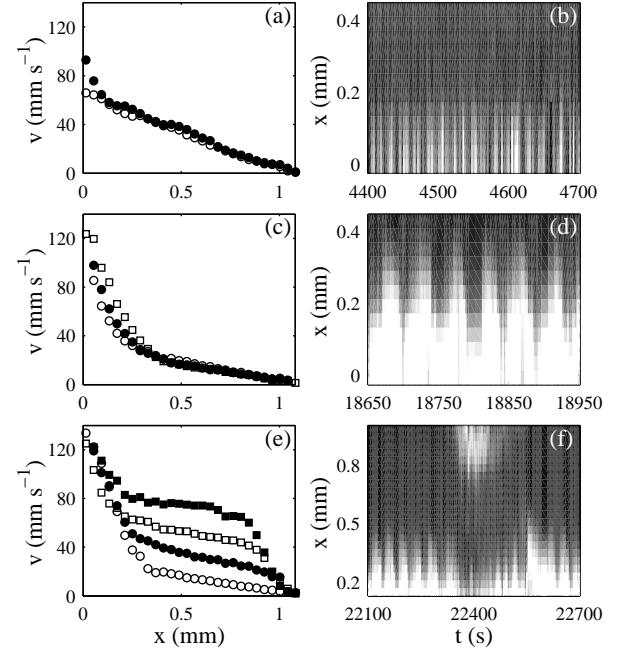


FIG. 4: Description of the fast dynamics. (a) Velocity profiles during the intermittent apparition of a highly sheared band at the rotor ($x \lesssim 150 \mu\text{m}$) at $t = 4505$ (\bullet), and 4508 s (\circ). (b) Enlargement of $\dot{\gamma}(x, t)$ over $t = 4400\text{--}4700 \text{ s}$. (c) Velocity profiles during one interface oscillation at $t = 18800$ (\circ), 18810 (\bullet), and 18818 s (\square). (d) Enlargement of $\dot{\gamma}(x, t)$ over $t = 18650\text{--}18950 \text{ s}$. (e) Velocity profiles during the nucleation of a second highly sheared band at $t = 22292$ (\circ), 22350 (\bullet), 22388 (\square), and 22463 s (\blacksquare). (f) Enlargement of $\dot{\gamma}(x, t)$ over $t = 22100\text{--}22700 \text{ s}$.

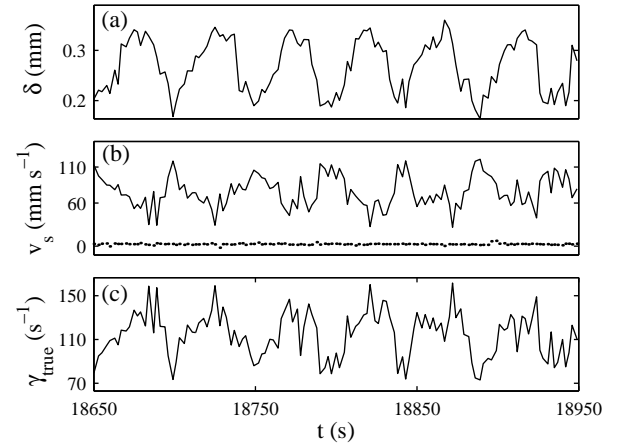


FIG. 5: Temporal fluctuations of (a) the position of the interface $\delta(t)$, (b) the slip velocities at the rotor $v_{s1}(t)$ (solid line) and at the stator $v_{s2}(t)$ (dotted line), and (c) the true shear rate $\dot{\gamma}_{\text{true}}(t)$, recorded during the oscillations of Fig. 4(d)

sheared band at the stator (see Fig. 4(e) and (f)). This phenomenon develops within roughly 200 s and takes place rather intermittently. According to Ref. [14], such a transient event is conceivable in Couette geometries of low enough curvature. On the spatio-temporal data $\dot{\gamma}(x, t)$, it shows up as a white patch for $x \gtrsim 0.8$ mm. This process seems to occur more frequently at the end of the experiment (see Fig. 2). Oscillations similar to those of Fig. 4(d) are clearly visible before and after the event of Fig. 4(f).

Let us conclude by discussing the main question raised by our study: what is the origin of the various time scales involved in the spatio-temporal dynamics of our micellar system? Concerning the *slow time scales*, the present results reveal a strong similarity with the evolution reported in Ref. [4]. However, our system is more than two orders of magnitude slower: “intermediate” and “long” times correspond respectively to 200–8000 s and 8000–24000 s here vs. 5–35 s and 35–175 s in Ref. [4]. Such a huge discrepancy could be explained by the differences in composition, electrostatic screening, or proximity to the I–N transition. In the framework of theoretical approaches derived from the Johnson-Segalman model [14], such long time scales mean that the diffusion coefficient D of the shear stress through the interface is vanishingly small. The interface speed is predicted to scale as $\sqrt{D}(\sigma - \sigma_\infty)$. The dashed line in Fig. 2 shows that our data are fairly compatible with this prediction.

Finally, the presence of *fast time scales* ranging from 5 to 50 s and thus strongly exceeding the micelle relaxation time $\tau_R \approx 40$ ms remains very puzzling [15]. Recent phenomenological models including dynamical equations for the micelle length and/or relaxation time predict oscillations and even chaotic-like states of the flow field that could be connected to the dynamics observed experimentally [16]. However, we believe that *wall slip dynamics* may play a major role in our experiments. Indeed, time scales of the same order have been found after small shear rate jumps between two banded states [17]. They were related to the interface reconstruction after band destabilization. Here, due to wall slip, the true shear rate is not stationary (see Fig. 5(c)). The interface could thus be periodically destabilized and reconstructed by the same process as in Ref. [17]. As a cause for the slip dynamics, one may invoke some multi-valuedness of the shear rate inside the lubricating layers at a given shear stress, which would lead to an instability near the walls similar to stick-slip or “spurt” effect [18]. Further studies will focus on trying to isolate the bulk behavior from that of sliding layers and determine how the two are coupled.

In summary, ultrasonic velocimetry allows the study of sheared complex fluids on time scales of about 1 s. Such a time resolution is crucial since a wrong picture of the flow may be deduced from velocity profiles averaged

on longer times with slower techniques. In the case of a wormlike micelle solution, various dynamical regimes were unveiled: the slow nucleation and growth of a shear band as well as more complex faster behaviors. These results, together with evidence for strong wall slip dynamics, demonstrate the importance of spatio-temporal fluctuations in shear-banded flows. More generally, they emphasize the need for time-resolved measurements as well as dynamical theoretical approaches in the study of complex fluid flows.

The authors wish to thank D. Anache and the “Cellule Instrumentation” of CRPP for technical help with the experiment. Fruitful discussions with A. Aradian, F. Molino, P. Olmsted, G. Porte, and J.-B. Salmon are acknowledged.

-
- [1] R. G. Larson, *The Structure and Rheology of Complex Fluids* (Oxford University Press, Oxford, 1999).
 - [2] *Soft and Fragile Matter: Non Equilibrium Dynamics Metastability and Flow*, edited by M. E. Cates and M. R. Evans (IOP, Bristol, U.K., 2000).
 - [3] E. Cappelaere *et al.*, Colloids Surfaces A, **104**, 353 (1995); Phys. Rev. E, **56**, 1869 (1997).
 - [4] S. Lerouge *et al.*, Phys. Rev. Lett., **81**, 5457 (1998); Langmuir, **16**, 6464 (2000).
 - [5] J.-F. Berret *et al.*, J. Phys. II France, **4**, 1261 (1994); V. Schmitt *et al.*, Langmuir, **10**, 955 (1994).
 - [6] J.-B. Salmon *et al.* Phys. Rev. Lett., **90**, 228303 (2003).
 - [7] M. M. Britton and P. T. Callaghan, Phys. Rev. Lett., **78**, 4930 (1997); Eur. Phys. J. B, **7**, 237 (1999).
 - [8] H. Rehage and H. Hoffmann, Mol. Phys., **74**, 933 (1991); J.-F. Berret *et al.*, Phys. Rev. E, **55** 1668 (1997).
 - [9] E. Fischer and P. T. Callaghan, Europhys. Lett., **50**, 803 (2000); Phys. Rev. E, **64**, 011501 (2001).
 - [10] R. W. Mair and P. T. Callaghan, J. Rheol., **41**, 901 (1997); W. M. Holmes *et al.*, Europhys. Lett., **64**, 274 (2003).
 - [11] S. Manneville *et al.*, submitted to Eur. Phys. J. AP, e-print cond-mat/0311072 (2003).
 - [12] C. Grand *et al.*, J. Phys. II France, **7**, 1071 (1997); J.-F. Berret and G. Porte, Phys. Rev. E, **60**, 4268 (1999); J.-F. Berret *et al.*, Europhys. Lett., **25**, 521 (1994).
 - [13] Animations of the velocity profiles are available at: <http://www.crpp-bordeaux.cnrs.fr/~sebm/usv>.
 - [14] O. Radulescu *et al.*, Rheol. Acta, **38**, 606 (1999).
 - [15] A mechanical effect, such as a small amount of wobble, would lead to a single time scale corresponding to the rotation period 0.75 s of the rotor. Moreover, in the system under study, $\dot{\gamma} = 200 \text{ s}^{-1}$ is far from any hydrodynamic or elastic instability.
 - [16] S. M. Fielding and P. D. Olmsted, e-print cond-mat/0310658 (2003); A. Aradian and M. E. Cates, e-print cond-mat/0310660 (2003).
 - [17] O. Radulescu *et al.*, Europhys. Lett., **62**, 230 (2003).
 - [18] J. L. A. Dubbeldam and J. Molenaar, J. Non-Newtonian Fluid Mech., **112**, 217 (2003).